Article

Measuring spin correlation between quarks during QCD confinement

https://doi.org/10.1038/s41586-025-09920-0

Received: 5 June 2025

Accepted: 14 November 2025

Published online: 4 February 2026

Open access

Check for updates

STAR Collaboration*

The vacuum is now understood to have a rich and complex structure, characterized by fluctuating energy fields[1] and a condensate of virtual quark–antiquark pairs. The spontaneous breaking of the approximate chiral symmetry[2], signalled by the nonvanishing quark condensate $\langle q\bar{q}\rangle$, is dynamically generated through topologically nontrivial gauge configurations such as instantons[3]. The precise mechanism linking the chiral symmetry breaking to the mass generation associated with quark confinement[4] remains a profound open question in quantum chromodynamics (QCD)—the fundamental theory of strong interaction. High-energy proton–proton collisions could liberate virtual quark–antiquark pairs from the vacuum that subsequently undergo confinement to form hadrons, whose properties could serve as probes into QCD confinement and the quark condensate. Here we report evidence of spin correlations in $\Lambda\bar{\Lambda}$ hyperon pairs inherited from spin-correlated strange quark–antiquark virtual pairs. Measurements by the STAR experiment at the Relativistic Heavy Ion Collider (RHIC) at Brookhaven National Laboratory reveal a relative polarization signal of (18 ± 4)% that links the virtual spin-correlated quark pairs from the QCD vacuum to their final-state hadron counterparts. Crucially, this correlation vanishes when the hyperon pairs are widely separated in angle, consistent with the decoherence of the quantum system. Our findings provide a new experimental model for exploring the dynamics and interplay of quark confinement and entanglement.

In our observable universe, hadrons, such as protons and neutrons, are among the fundamental building blocks of matter that form the physical world. Hadrons are not fundamental particles but composite systems made up of quarks and gluons, collectively referred to as partons. One of nature's most profound phenomena is that partons cannot exist as free particles. Instead, the strong force confines partons into hadrons—a phenomenon known as confinement[4].

More rigorously, confinement arises from the disordering of gauge fields at large distances, such that vacuum fluctuations of the chromodynamic fields confine colour flux into narrow tubes. Simply put, this mechanism produces a linearly rising potential between static quarks and ensures the absence of coloured asymptotic states. This can be essentially illustrated as pulling two quarks apart to a certain distance at which, instead of breaking the quarks, more quarks are created.

The Higgs boson, discovered in 2012 at the Large Hadron Collider[5,6], was the final missing piece of the Standard Model[7] and helps to explain the origin of mass for fundamental particles such as quarks and leptons. Notably, light quarks by themselves have masses of only several MeV c^{-2}, yet protons and neutrons—each composed of just three valence quarks (up and down) bound by massless gluons—have masses on the order of 1 GeV c^{-2}, making them about 150 times more massive. Where does most of the hadron mass come from? Similarly, the spin structure of the proton presents another puzzle: experimental measurements indicate that quark contributions account for only about 35% of the total proton spin[8], in strong contrast to the expectation from the SU(6) quark model[9], which predicts that 100% of the spin arises from valence quarks. The fundamental question is to understand the origin of these emergent hadron structures, for example, mass and spin, which arise as a consequence of quark confinement.

QCD[10], the theory of strong interactions, exhibits asymptotic freedom in which partons interact weakly in short distances. The absence of such asymptotic states at large distances, for example, the length scale of a hadron approximately 1 fm (10^{-15} m), leads to the quark confinement. To understand this, however, the complexity of first-principles QCD calculations becomes difficult to solve numerically at present computational power, owing to the nature of low-energy self-interacting gluons. This challenging regime, in which simple approximations no longer work, is called nonperturbative QCD. Therefore, the detailed mechanisms through which confinement occurs from partons to hadrons, and how it manifests itself in hadron structure, remain unresolved puzzles[11].

Analysis method

We introduce a new experimental approach to investigate quark confinement by studying parton evolution and the transition of virtual quarks from the QCD vacuum to final-state hadrons. Similar to the Higgs mechanism, chiral symmetry is spontaneously broken in the

*A list of authors and their affiliations appears at the end of the paper.

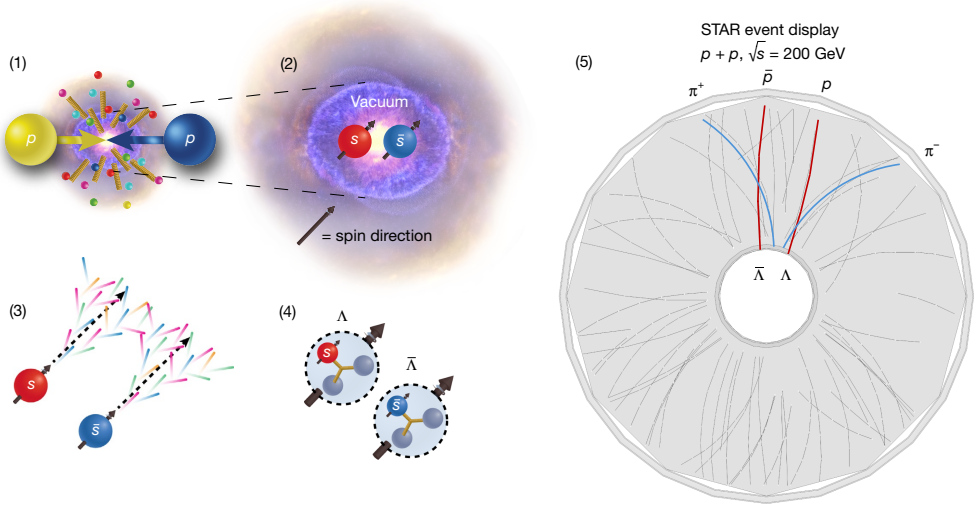

Fig. 1 | Exciting the vacuum in high-energy proton–proton collisions. Illustration of tracing the QCD evolution of the spin of a strange quark–antiquark pair to a $\Lambda\overline{\Lambda}$ hyperon pair and how it can be measured by the STAR experiment at RHIC. See (1)–(5) in the text for details.

QCD vacuum at zero temperature. It is expected that there are similar numbers of virtual up (u), down (d) and strange (s) quark pairs[12] forming the quark condensate.

Owing to the quantum numbers of the vacuum, $J^{PC} = 0^{++}$, in which J, P and C represent total angular momentum, parity and charge conjugation, respectively, a strong constraint is imposed on the spin configuration of quark–antiquark pairs from the chiral condensate. As a result, these pairs are expected to have their spins parallel[12] in their rest frame, which means that they are in spin-triplet states. Thanks to high-energy proton–proton collisions, these virtual quark–antiquark pairs from the vacuum can be liberated and materialize into real particles. Besides other strong experimental indications in hadron spectroscopy[13,14] and lattice QCD calculations[15], observing the correlated pairs from the vacuum in spin-triplet states can be direct experimental evidence of the quark condensate.

Alternatively, depending on the choice of final-state particles, quark–antiquark pairs can also arise from virtual gluon splitting, that is, $g \to q\bar{q}$. This process is expected to play a more substantial role in the high-energy regime (also known as the perturbative regime)[16], offering complementary insights into hadronization. Nevertheless, understanding the transition from quark pairs to final-state hadrons remains essential for tackling the fundamental problem of quark confinement.

Specifically, our approach is as follows:

1. Protons are accelerated to 99.996% of the speed of light for collisions that excite the QCD vacuum[17] and liberate quark pairs from the condensate.
2. Of these quark pairs, there are strange quark–antiquark ($s\bar{s}$) pairs with their spins parallel, that is, in spin-triplet states[12,16].
3. Owing to confinement, the liberated quarks cannot exist independently. Each quark of the $s\bar{s}$ pair will undergo the quark-to-hadron transition, known as hadronization.
4. Some $s\bar{s}$ pairs hadronize into Λ and $\overline{\Lambda}$ hyperon pairs, in which a Λ hyperon has one strange (s), one up (u) and one down (d) quark. (The structure of the $\overline{\Lambda}$ hyperon is similar but using the antiquarks). The Λ hyperon is a spin-1/2 hadron with a lifetime of about 10^{-10} s, for which the spin polarization can be measured through the decay kinematics and direction of the momentum vector of the daughter particles[18], that is, proton and pion. From the nonrelativistic SU(6) quark model[9], the spin of the Λ hyperon is carried 100% by the strange quark.
5. These decay particles, along with other particles, can be measured by the STAR detector. The reconstruction of the decay daughters can provide the spin polarization of the Λ and $\overline{\Lambda}$ hyperons, which then allows determination of the hyperon pair spin correlation. An illustration of this approach is shown in Fig. 1.

This method makes use of the spin correlation of $\Lambda\overline{\Lambda}$ hyperon pairs and compares them with their quark-level counterparts. At the moment of $s\bar{s}$ production, the relative spin orientation of the pair is expected to be parallel. During hadronization, these quarks interact with the surrounding QCD environment to form Λ and $\overline{\Lambda}$ hyperons. The innovation of this approach lies in observing the degree of (de)coherence of the correlated $s\bar{s}$ pairs as they transition into hadrons. The quantitative measurement of this (de)coherence provides direct insights into the nonperturbative process of quark-to-hadron transitions, which is challenging for first-principles QCD calculations to address. Tracing this dynamical loss of quantum coherence during hadronization represents a new model for exploring QCD phenomena.

Experiment

This measurement is performed at the Solenoidal Tracker at RHIC (STAR) detector[19]. Charged-particle tracking, including transverse momentum reconstruction and charge sign determination, is provided by the time projection chamber (TPC) positioned in a 0.5-T solenoidal magnetic field. The TPC volume extends radially from 50 to 200 cm from the beam axis and covers pseudorapidities $|\eta| < 1.0$ over the full azimuthal angle, $0 < \phi < 2\pi$. (Pseudorapidity is a kinematic variable related to the angle (θ) between the particle's momentum and the positive beam axis as, $\eta = -\ln(\tan(\theta/2))$. For example, $\eta = 1$ corresponds to $\theta \approx 40°$). The TPC also provides energy loss per unit length (dE/dx) measurement of tracks used for particle identification.

This measurement was conducted in proton–proton ($p + p$) collisions at the centre-of-mass energy $\sqrt{s} = 200$ GeV, using a dataset collected in 2012 by the STAR detector at RHIC. All three combinations, $\Lambda\overline{\Lambda}$, $\Lambda\Lambda$ and $\overline{\Lambda}\overline{\Lambda}$, are reported. The data are measured in the two-particle separation in rapidity, Δy, and azimuthal angle, $\Delta\phi$, respectively. Here rapidity y is a variable that describes velocity along the beam direction ($y = 1/2\ln((E + p_z)/(E - p_z))$). Data from $K^0_S K^0_S$ spin correlations and simulations from the PYTHIA 8.3 Monte Carlo (MC) model[20] are compared with the Λ measurement and used as a baseline reference. No spin correlation is expected from either of them, as K^0_S are scalar (spin-0) mesons and no Λ hyperon spin physics is included in the

PYTHIA 8.3 MC model. The signal extraction method for $K_S^0K_S^0$ pairs is the same as for Λ hyperon pairs.

Data analysis

Only events with a primary vertex within 60 cm from the centre of the STAR detector along the proton beam axis were accepted for further analysis. A total of about 600 million minimum-bias $p+p$ events were selected and analysed, requiring the coincidence of STAR Vertex Position Detectors, which are located on the upstream and downstream ends of the detector.

The Λ and $\overline{\Lambda}$ hyperons are reconstructed by means of their hadronic decay $\Lambda \to p\pi^-$ ($\overline{\Lambda} \to \overline{p}\pi^+$). The selection of $\Lambda\overline{\Lambda}$, ΛΛ and $\overline{\Lambda}\overline{\Lambda}$ pairs is done on the basis of a 2D Gaussian fit to the 2D invariant mass ($M_{\rm inv}$) distributions of the $p\pi$ pairs. Only Λ and $\overline{\Lambda}$ hyperon candidates that are at mid-rapidity ($|y|<1$), with transverse momentum $p_{\rm T}$ within $0.5<p_{\rm T}<5.0$ GeV c^{-1}, are selected for the analysis. The average transverse momentum $\langle p_{\rm T,\Lambda}\rangle$ of reconstructed Λ hyperons is 1.35 GeV c^{-1}.

On the basis of PYTHIA 8.2 (ref. 21) and STAR detector simulation, only 11% of measured $\Lambda\overline{\Lambda}$ pairs contain primary Λ and $\overline{\Lambda}$ hyperons. The remaining 89% of the pairs have at least one Λ or $\overline{\Lambda}$ hyperon from the decay of a higher-mass particle. The impact of this so-called feed-down contribution is included in the model calculations when compared with data (Methods).

Measurement of spin correlations

After selecting the signal Λ pairs, the decay (anti)protons are boosted into the rest frames of their parent particles and the opening angle θ^* between the two boosted (anti)protons is determined. Such (anti)proton pairs are expected to follow the angular distribution[22–24]:

$$\frac{1}{N}\frac{{\rm d}N}{{\rm d}\cos\theta^*}=\frac{1}{2}[1+\alpha_1\alpha_2 P_{\Lambda_1\Lambda_2}\cos\theta^*], \quad (1)$$

in which $P_{\Lambda_1\Lambda_2}$ is the spin correlation signal or the relative polarization of the Λ hyperon pair and α_1 and α_2 are the weak decay parameters of the Λ ($\alpha_-=0.747\pm0.009$) or $\overline{\Lambda}$ ($\alpha_+=-0.757\pm0.004$) (ref. 7). For parallel spins, we expect $P_{\Lambda_1\Lambda_2}=1/3$, whereas for antiparallel spins $P_{\Lambda_1\Lambda_2}=-1$ and for no spin correlation $P_{\Lambda_1\Lambda_2}=0$.

The dN/dcosθ^* distribution is constructed for both the total hyperon pairs, which includes signal and background, and the background-only hyperon pairs. Before the signal can be extracted, the raw dN/dcosθ^* distributions were corrected for detector acceptance loss and inefficiency. The correction was performed using the mixed-event (ME) technique for all dN/dcosθ^* distributions.

The details of the Λ reconstruction, signal extraction and the ME corrections are described in Methods.

In Fig. 2, the corrected dN/dcosθ^* signal distributions for $\Lambda\overline{\Lambda}$, ΛΛ and $\overline{\Lambda}\overline{\Lambda}$ are shown. The top and bottom panels show the spin correlations for short-range ($|\Delta y|<0.5$ and $|\Delta\phi|<\pi/3$) and long-range ($0.5<|\Delta y|<2.0$ and/or $\pi/3<|\Delta\phi|<\pi$) Λ pairs, respectively. The lines are the linear fits to the data according to equation (1). Quality of the fits used for signal extraction is discussed in Methods.

Figure 3 shows the Λ hyperon spin correlations, expressed in terms of the value of $P_{\Lambda_1\Lambda_2}$, for short-range (left) and long-range (right) pairs. We found that the short-range $\Lambda\overline{\Lambda}$ pairs show a positive spin correlation of $P_{\Lambda\overline{\Lambda}}=0.181\pm0.035_{\rm stat}\pm0.022_{\rm sys}$, with a 4.4 standard deviation significance with respect to zero. For details about the systematic uncertainties, see Methods. The short-range ΛΛ and $\overline{\Lambda}\overline{\Lambda}$ pairs and all long-range pairs exhibit spin correlation consistent with zero. The $K_S^0K_S^0$ measurements and PYTHIA 8.3 predictions are shown for comparison and are consistent with zero for both short-range and long-range pairs, as expected. This result marks the first evidence of a positive spin correlation between Λ and $\overline{\Lambda}$ in high-energy $p+p$ collisions.

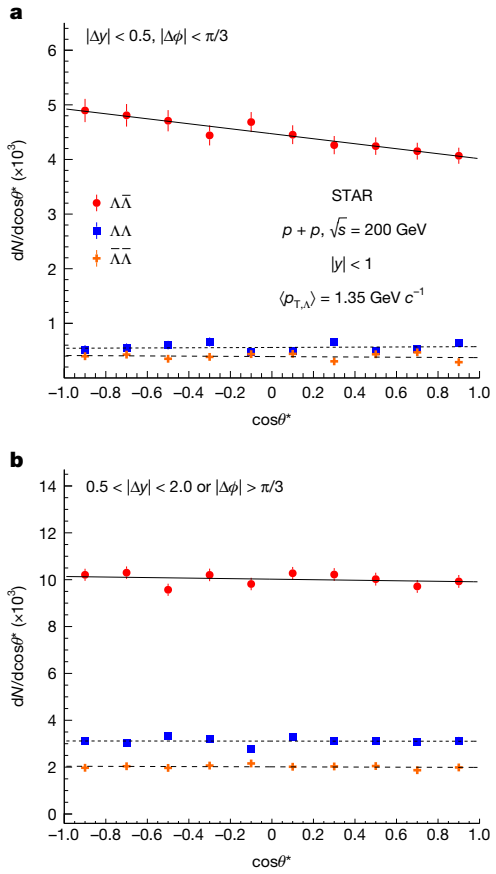

Fig. 2 | Self-analysing Λ hyperons reveal polarization through decays. dN/dcosθ^* distributions of decay (anti)protons for $\Lambda\overline{\Lambda}$, ΛΛ and $\overline{\Lambda}\overline{\Lambda}$ hyperon pairs measured at mid-rapidity ($|y|<1$). **a**, Short-range pairs ($|\Delta y|<0.5$ and $|\Delta\phi|<\pi/3$). **b**, Long-range pairs. Statistical uncertainties are denoted by the error bars. The fits to the data represented by lines are used to demonstrate the magnitude of the spin–spin correlation.

The positive polarization of short-range $\Lambda\overline{\Lambda}$ pairs corresponds to a parallel spin configuration[25], for which this orientation of the spin is expected from the chiral condensate $\langle q\overline{q}\rangle\neq0$ (ref. 12). An alternative scenario—gluons splitting into $s\overline{s}$ pairs—has also been investigated. According to the PYTHIA 8.3 prediction, we found negligible contributions from this process for pairs within our measured momentum range. Furthermore, hadronic final-state interaction has been investigated by means of a femtoscopic-type correlator[26], which is found to be negligible. Therefore, the observed spin correlation is strong evidence for the presence of vacuum quark pairs originating from the chiral condensate.

We have studied the pair kinematic dependence of this spin correlation to further understand the underlying spin correlation. As the separation of the pairs, characterized by $\Delta R=\sqrt{\Delta y^2+\Delta\phi^2}$, increases, the spin correlation of $\Lambda\overline{\Lambda}$ is found to be weaker, as shown in Fig. 4. Also, we compare the results with model calculations in conjunction with the feed-down contributions of Λs based on prediction from PYTHIA 8.2 and STAR detector simulation.

Although the maximum relative polarization correlation of the spin-parallel $s\overline{s}$ pair is $P_{\Lambda_1\Lambda_2}=1/3$ (ref. 24), with the feed-down contributions, for example, from Σ^0 and other strange baryons, the correlation for $\Lambda\overline{\Lambda}$ pairs is expected to be less than 1/3. The expected $\Lambda\overline{\Lambda}$ spin correlation from the SU(6) model is found to be (9.6 ± 0.4)% with our data kinematic selections (Methods). The model calculation has no interaction mechanism, so the results only reflect the correlation on the hadron level assuming that the initial strange quark pairs are still 100%

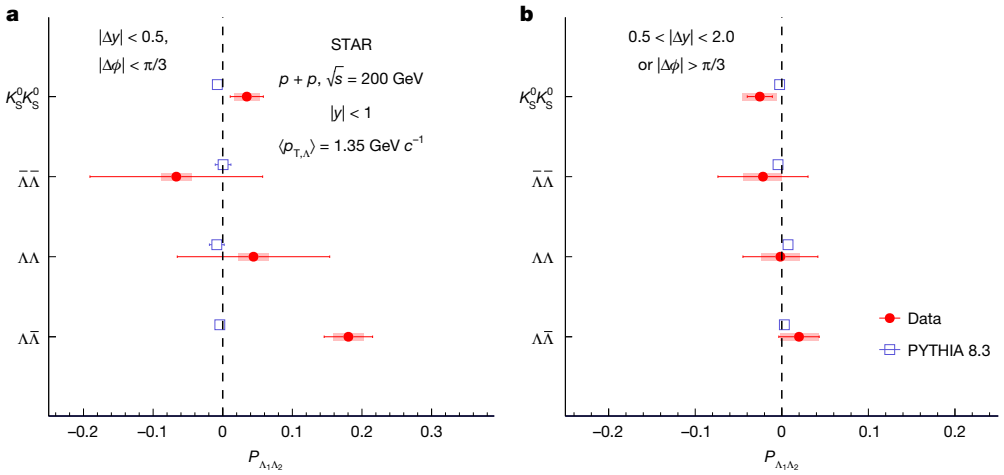

Fig. 3 | Comparison between data spin correlations with the MC model. Spin correlation $P_{\Lambda_1\Lambda_2}$ of short-range (**a**) and long-range (**b**) $\Lambda\bar{\Lambda}$, $\Lambda\Lambda$ and $\bar{\Lambda}\bar{\Lambda}$ hyperon pairs. The hyperon pair $P_{\Lambda_1\Lambda_2}$ is compared with $K^0_S K^0_S$ measurements and PYTHIA 8.3 predictions. Statistical uncertainties are denoted by the error bars and the systematic uncertainties are represented by the shaded boxes.

spin aligned. We find that the data are compatible with the SU(6) quark model, with 100% spin aligned $s\bar{s}$ pairs in the initial state, within the uncertainty at small ΔR. The Burkardt–Jaffe model predicts smaller polarization[27] and is disfavoured by our data. The detailed calculations of these models, as well as the PYTHIA 8 simulations for feed-down contributions, are included in Methods.

Our result shows a large spin correlation at small ΔR but a correlation consistent with zero at large ΔR. This suggests that: (1) within uncertainties, the spin correlation of short-range $\Lambda\bar{\Lambda}$ pairs are at their maximal values, consistent with inheriting 100% from their $s\bar{s}$ counterparts at the quark level; (2) decoherence effects from quark and gluon interactions or several initial $s\bar{s}$ pairs might have diluted, if not washed out, the spin correlations when the pairs are widely separated. We expect that both findings will contribute to our understanding of QCD evolution and quark-to-hadron transitions.

In terms of entanglement measures, for example, the Peres–Horodecki criterion or positive partial transpose (PPT) test[28,29], the case of spin-triplet $\Lambda\bar{\Lambda}$ states warrants further detailed investigation. In particular, it is important to evaluate both the isotropic two spin-1/2 configuration, for which the separability bound can be expressed in terms of a single correlation parameter, and the more general case that requires a full correlation-tensor analysis in the PPT framework. From the experimental side, extra care is also needed to quantify possible feed-down effects that could influence the observed spin correlations.

Similar measurements were performed in the past at experiment PS185 at LEAR, in which spin-triplet states were observed in the exclusive reaction $\bar{p}p \to \Lambda\bar{\Lambda}$ (refs. 30,31). This fixed-target experiment was conducted with an antiproton beam at approximately 1.7 GeV c^{-1}, featuring kinematics that are very different from those in this study. Moreover, the spin correlation was measured by means of a global axis, that is, with respect to the production plane. At the present STAR kinematics, global polarization is not expected[32]. This was verified by measuring the spin–spin correlation of $\Lambda\bar{\Lambda}$ pairs that are close in ϕ and far in y ($|\Delta\phi| < \pi/3$, $|\Delta y| > 0.6$). No spin–spin correlation is observed for such pairs, with $P_{\Lambda\bar{\Lambda}} = -0.012 \pm 0.073_{\text{stat}} \pm 0.022_{\text{sys}}$, which indicates that the observed spin–spin correlation for short-range $\Lambda\bar{\Lambda}$ pairs is not a result of correlation of Λ and $\bar{\Lambda}$ to common global production plane. Establishing the exact connection, however, remains an interesting subject for future investigation in collaboration with theoretical studies. Other noteworthy measurements, similar to ours, are those by the BES III Collaboration, which used hyperon spin correlations to look for CP symmetry violation signals in J/ψ decay[33,34].

Discussion and applications

QCD confinement and chiral symmetry breaking

In QCD, confinement and spontaneous chiral symmetry breaking are rigorously defined phenomena[2,4] and our very existence is, in a sense, a testament to their reality. What remains less well understood, however, is their role in the formation of hadrons—the transition from quarks to bound states—and how fundamental properties such as mass and spin emerge in this process.

In this work, we present a new experimental approach to study the evolution of spin correlation during the nonperturbative hadronization process. To our knowledge, for the first time, we trace the spin degrees of freedom of a quark–antiquark pair as it evolves into hadrons, demonstrating that most, if not all, of the original partonic spin polarization is preserved through hadronization. By using quark's initial spin correlation, the new experimental approach may provide a more direct probe of the quark condensate to study QCD vacuum structure, for example, topological charge fluctuations, local strong charge-conjugate and parity violation and so on. One immediate implication is to discover whether chiral symmetry can be restored (see later section 'Chiral symmetry restoration'). This finding provides a valuable new probe for lattice QCD calculations and for future quantum computing approaches aimed at unravelling the nonperturbative dynamics of confinement.

Spin decomposition

The reported result provides direct experimental insight into how much spin the strange quark can contribute to the Λ spin. The result favours the nonrelativistic SU(6) quark model, leaving little room for contributions from gluons and orbital angular momentum. This is counter-intuitive given the famous 'proton spin crisis'[35], which suggests that valence quarks only contribute about 35% of the proton spin. STAR has experimentally confirmed that about half of the remaining 65% originates from gluons[36,37]. Does the hyperon spin structure exhibit a different decomposition to that of protons? In any scenario, the answer will be important for understanding nonperturbative QCD.

Λ polarization puzzle

One of the outstanding puzzles in nuclear and particle physics is the large transverse Λ polarization in unpolarized collisions[18]. Over the past 50 years, the question 'How does the Λ hyperon obtain its spin?' has been extensively debated. See ref. 38 for further discussions. The reported result provides a new experimental constraint to validate both initial-state and final-state driven models, especially because the

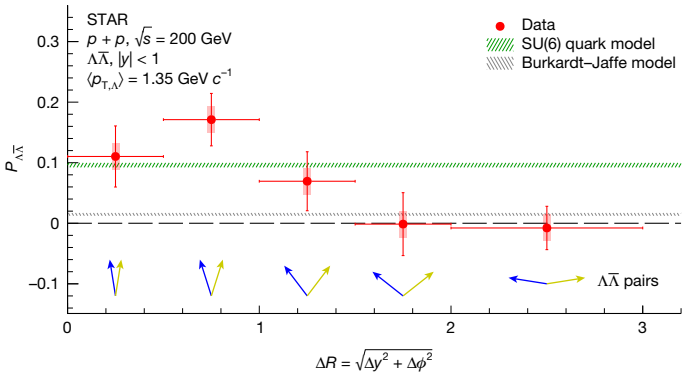

Fig. 4 | Angular dependence of $\Lambda\bar{\Lambda}$ spin correlations. Spin correlation $P_{\Lambda_1\Lambda_2}$ as a function of pair separation ΔR. The data are compared with predictions from the SU(6) quark model[9] and the Burkardt–Jaffe model[27]. Statistical uncertainties are denoted by the error bars and the systematic uncertainties are represented by the shaded boxes. The blue and yellow arrows are used to illustrate the separation of the $\Lambda\bar{\Lambda}$ pairs.

large transverse polarization has been observed in Λ production but not $\bar{\Lambda}$ production[39].

Spin transfer

This experimental approach provides valuable insights into spin-transfer measurements carried out in the past[40–43] to measure the quark helicity and transversity distributions (how much of the longitudinal and transverse polarization of the proton propagates to its quarks, respectively). For more information about these distributions, see ref. 44.

Orbital angular momentum

Owing to quantum numbers of the vacuum, the orbital angular momentum state $L = 1$ is expected for the $s\bar{s}$ pairs. From the final-state hyperons, we can measure the momentum distribution in the centre-of-mass frame of the pair, for which the scenarios of $L = 0$ and $L = 1$ would exhibit different momentum dependence[9]. This is of great interest for future measurements and may link to the problem of quark orbital angular momentum inside the proton.

Quantum decoherence

We find that the kinematic dependence of the $\Lambda\bar{\Lambda}$ spin correlations may reveal quantum decoherence effects in the $p + p$ collision system. We know that there is entanglement from top quark pairs[45,46]. In this case, the initial state $s\bar{s}$ pairs could be in a mixed triplet state, which may require a general PPT test that goes beyond just measuring the relative polarization, to perform the entanglement measure. Nonetheless, using pairs measured after hadronization and going from short-range to long-range pairs, the relative reduction in spin correlation may be sensitive to quantum decoherence effect from the initial states. Similarly, according to ref. 22, building on Tornqvist's work[23,24], this could test Bell's inequality and pair nonlocality to study QCD string spin dynamics. This leads a new model for exploring hadronization in the context of quantum information science and the quantum-to-classical transitions[47].

Chiral symmetry restoration

At high temperatures, QCD matter—such as the quark–gluon plasma—is expected to undergo chiral symmetry restoration owing to the disappearance of the quark condensate. However, experimental evidence for this phenomenon in heavy-ion collisions remains inconclusive[48–54]. The observation of a distinct $\Lambda\bar{\Lambda}$ spin correlation, particularly in spin singlet states (for example, $^1S_0$)[16], could serve as a new experimental probe for investigating quark–gluon plasma dynamics.

Among future opportunities, one of the most important steps in further understanding the QCD evolution from parton spins to hadron spins is the experimental control of the quark–antiquark spin configuration and its origins. As discussed earlier, the low transverse momentum region is sensitive to the chiral condensate in the QCD vacuum, in which $s\bar{s}$ pairs are expected to be 100% spin aligned. However, as the Λ momentum increases, the gluon splitting process, $g \to s\bar{s}$, becomes more important. This momentum dependence will be of great interest in the future. Experimental measurements can further constrain these scenarios to higher Λ hyperon momentum, to Λ as a fragment of a high-momentum parton (called jet) or to higher rapidities and/or centre-of-mass energies. Also, momentum correlation function studies[55–57] in conjunction with spin correlations (this work) between Λ hyperons (or with other hyperons) can be carried out to explore hadronic final-state interactions, especially in heavy-ion collisions. All of the above directions are promising possibilities in the STAR experiment.

Summary

We present the first evidence for spin correlations with Λ hyperon pairs in high-energy $p + p$ collisions at RHIC, measured across different kinematic regimes. Notably, among all possible combinations of Λ hyperon pairs, short-range $\Lambda\bar{\Lambda}$ pairs exhibit a near-maximal expected relative polarization, $P_{\Lambda\bar{\Lambda}} = 0.181 \pm 0.035_{\text{stat}} \pm 0.022_{\text{sys}}$, with a significance of 4.4 standard deviations. As separation of the pair increases, the spin correlation decreases substantially, probably because of quantum decoherence or other interaction mechanisms. By examining the QCD evolution of a strange quark–antiquark pair that is expected to be spin aligned from the vacuum condensate, this new hadron-level measurement provides insights into the underlying mechanisms of QCD confinement. The observation of this relative polarization, alongside the methodology established for spin correlation measurements of hyperon pairs, paves the way for a transformative approach to understanding the complex dynamics of QCD.

Online content

Any methods, additional references, Nature Portfolio reporting summaries, source data, extended data, supplementary information, acknowledgements, peer review information; details of author contributions and competing interests; and statements of data and code availability are available at https://doi.org/10.1038/s41586-025-09920-0.

1. Weinberg, S. The cosmological constant problem. *Rev. Mod. Phys.* **61**, 1 (1989).
2. Nambu, Y. & Jona-Lasinio, G. Dynamical model of elementary particles based on an analogy with superconductivity. I. *Phys. Rev.* **122**, 345 (1961).
3. Schäfer, T. & Shuryak, E. V. Instantons in QCD. *Rev. Mod. Phys.* **70**, 323 (1998).
4. Greensite, J. *An Introduction to the Confinement Problem* (Springer, 2011).
5. Chatrchyan, S. et al. Observation of a new boson at a mass of 125 GeV with the CMS experiment at the LHC. *Phys. Lett. B* **716**, 30–61 (2012).
6. Aad, G. et al. Observation of a new particle in the search for the Standard Model Higgs boson with the ATLAS detector at the LHC. *Phys. Lett. B* **716**, 1–29 (2012).
7. Navas, S. et al. Review of particle physics. *Phys. Rev. D* **110**, 030001 (2024).
8. Ashman, J. et al. A measurement of the spin asymmetry and determination of the structure function g_1 in deep inelastic muon-proton scattering. *Phys. Lett. B* **206**, 364–370 (1988).
9. Riazuddin, F. *A Modern Introduction to Particle Physics* 159–180 (World Scientific, 2011).
10. Gross, D. J. & Wilczek, F. Ultraviolet behavior of non-abelian gauge theories. *Phys. Rev. Lett.* **30**, 1343 (1973).
11. Accardi, A. et al. Electron Ion Collider: the next QCD frontier. *Eur. Phys. J. A* **52**, 268 (2016).
12. Ellis, J., Kharzeev, D. & Kotzinian, A. The proton spin puzzle and Λ polarization in deep-inelastic scattering. *Z. Phys. C* **69**, 467–474 (1995).
13. Gell-Mann, M., Oakes, R. J. & Renner, B. Behavior of current divergences under $SU_3 \times SU_3$. *Phys. Rev.* **175**, 2195 (1968).
14. Leutwyler, H. The masses of the light quarks. Preprint at https://arxiv.org/abs/hep-ph/9602255 (1996).
15. Hagler, P. Hadron structure from lattice quantum chromodynamics. *Phys. Rep.* **490**, 49–175 (2010).
16. Ellis, J. & Hwang, D. S. Spin correlations of $\Lambda\bar{\Lambda}$ pairs as a probe of quark–antiquark pair production. *Eur. Phys. J. C* **72**, 1877 (2012).

17. Peskin, M. E. & Schroeder, D. V. *An Introduction to Quantum Field Theory* (Addison-Wesley, 1995).
18. Bunce, G. et al. Λ^0 hyperon polarization in inclusive production by 300-GeV protons on beryllium. *Phys. Rev. Lett.* **36**, 1113 (1976).
19. Ackermann, K. H. et al. STAR detector overview. *Nucl. Instrum. Methods Phys. Res. A* **499**, 624–632 (2003).
20. Bierlich, C. et al. A comprehensive guide to the physics and usage of PYTHIA 8.3. *SciPost Phys. Codeb.* https://doi.org/10.21468/SciPostPhysCodeb.8 (2022).
21. Sjöstrand, T. et al. An introduction to PYTHIA 8.2. *Comput. Phys. Commun.* **191**, 159–177 (2015).
22. Gong, W., Parida, G., Tu, Z. & Venugopalan, R. Measurement of Bell-type inequalities and quantum entanglement from Λ-hyperon spin correlations at high energy colliders. *Phys. Rev. D* **106**, L031501 (2022).
23. Tornqvist, N. A. Suggestion for Einstein-Podolsky-Rosen experiments using reactions like $e^+e^- \to \Lambda\overline{\Lambda} \to \pi^-p\pi^+\overline{p}$. *Found. Phys.* **11**, 171–177 (1981).
24. Tornqvist, N. A. The decay $J/\psi \to \Lambda\overline{\Lambda} \to \pi^-p\pi^+\overline{p}$ as an Einstein-Podolsky-Rosen experiment. *Phys. Lett. A* **117**, 1–4 (1986).
25. Alexander, G. et al. A first measurement of the $\Lambda\overline{\Lambda}$ and $\Lambda\Lambda$ ($\Lambda\overline{\Lambda}$) spin compositions in hadronic Z^0 decays. *Phys. Lett. B* **384**, 377–387 (1996).
26. Baym, G. The physics of Hanbury Brown–Twiss intensity interferometry: from stars to nuclear collisions. *Acta Phys. Polon. B* **29**, 1839 (1998).
27. Burkardt, M. & Jaffe, R. L. Polarized $q \to \Lambda$ fragmentation functions from $e^+e^- \to \Lambda + X$. *Phys. Rev. Lett.* **70**, 2537 (1993).
28. Peres, A. Separability criterion for density matrices. *Phys. Rev. Lett.* **77**, 1413 (1996).
29. Horodecki, P. Separability criterion and inseparable mixed states with positive partial transposition. *Phys. Lett. A* **232**, 333–339 (1997).
30. Barnes, P. D. et al. From $\overline{p}p \to \Lambda\overline{\Lambda}$ with PS185 at LEAR. *Nucl. Phys. A* **558**, 277–286 (1993).
31. Paschke, K. D. et al. Experimental determination of the complete spin structure for $\overline{p}p \to \overline{\Lambda}\Lambda$ at $p\overline{p} = 1.637$ GeV/*c*. *Phys. Rev. C* **74**, 015206 (2006).
32. Aad, G. et al. Measurement of the transverse polarization of Λ and $\overline{\Lambda}$ hyperons produced in proton-proton collisions at $\sqrt{s} = 7$ TeV using the ATLAS detector. *Phys. Rev. D* **91**, 032004 (2015).
33. Ablikim, M. et al. Probing CP symmetry and weak phases with entangled double-strange baryons. *Nature* **606**, 64–69 (2022).
34. Ablikim, M. et al. Polarization and entanglement in baryon–antibaryon pair production in electron–positron annihilation. *Nat. Phys.* **15**, 631–634 (2019).
35. Hansson, J. The "proton spin crisis" - a quantum query. Preprint at https://arxiv.org/abs/hep-ph/0304225 (2003).
36. Abdallah, M. S. et al. Longitudinal double-spin asymmetry for inclusive jet and dijet production in polarized proton collisions at $\sqrt{s} = 510$ GeV. *Phys. Rev. D* **105**, 092011 (2022).
37. Adamczyk, L. et al. Precision measurement of the longitudinal double-spin asymmetry for inclusive jet production in polarized proton collisions at $\sqrt{s} = 200$ GeV. *Phys. Rev. Lett.* **115**, 092002 (2015).
38. Tu, Z. Deep exclusive meson production as a probe to the puzzle of Λ hyperon polarization. *Phys. Rev. C* **109**, 055205 (2024).
39. Airapetian, A. et al. Transverse polarization of Λ and $\overline{\Lambda}$ hyperons in quasireal photoproduction. *Phys. Rev. D* **76**, 092008 (2007).
40. Adam, J. et al. Transverse spin transfer to Λ and $\overline{\Lambda}$ hyperons in polarized proton-proton collisions at $\sqrt{s} = 200$ GeV. *Phys. Rev. D* **98**, 091103 (2018).
41. Abelev, B. I. et al. Longitudinal spin transfer to Λ and $\overline{\Lambda}$ hyperons in polarized proton-proton collisions at $\sqrt{s} = 200$ GeV. *Phys. Rev. D* **80**, 111102 (2009).
42. Abdulhamid, M. I. et al. Longitudinal and transverse spin transfer to Λ and $\overline{\Lambda}$ hyperons in polarized $p + p$ collisions at $\sqrt{s} = 200$ GeV. *Phys. Rev. D* **109**, 012004 (2024).
43. Alekseev, M. et al. Measurement of the longitudinal spin transfer to Λ and $\overline{\Lambda}$ hyperons in polarised muon DIS. *Eur. Phys. J. C* **64**, 171–179 (2009).
44. Boussarie, R. et al. TMD handbook. Preprint at https://arxiv.org/abs/2304.03302 (2023).
45. Aad, G. et al. Observation of quantum entanglement with top quarks at the ATLAS detector. *Nature* **633**, 542–547 (2024).
46. Hayrapetyan, A. et al. Observation of quantum entanglement in top quark pair production in proton–proton collisions at $\sqrt{s} = 13$ TeV. *Rep. Prog. Phys.* **87**, 117801 (2024).
47. Schlosshauer, M. The quantum-to-classical transition and decoherence. Preprint at https://arxiv.org/abs/1404.2635 (2014).
48. Khachatryan, V. et al. Observation of charge-dependent azimuthal correlations in *p*–Pb collisions and its implication for the search for the chiral magnetic effect. *Phys. Rev. Lett.* **118**, 122301 (2017).
49. Sirunyan, A. M. et al. Constraints on the chiral magnetic effect using charge-dependent azimuthal correlations in *p*Pb and PbPb collisions at the CERN Large Hadron Collider. *Phys. Rev. C* **97**, 044912 (2018).
50. Acharya, S. et al. Constraining the magnitude of the Chiral Magnetic Effect with Event Shape Engineering in Pb–Pb collisions at $\sqrt{s_{NN}} = 2.76$ TeV. *Phys. Lett. B* **777**, 151–162 (2018).
51. Abdallah, M. et al. Search for the chiral magnetic effect with isobar collisions at $\sqrt{s_{NN}} = 200$ GeV by the STAR Collaboration at the BNL Relativistic Heavy Ion Collider. *Phys. Rev. C* **105**, 014901 (2022).
52. Sung, H.-S. et al. K_s/K^* enhancement as a signature of chiral symmetry restoration in heavy ion collisions. *Phys. Lett. B* **819**, 136388 (2021).
53. Nishi, T. et al. Chiral symmetry restoration at high matter density observed in pionic atoms. *Nat. Phys.* **19**, 788–793 (2023).
54. Rapp, R. & Wambach, J. Chiral symmetry restoration and dileptons in relativistic heavy-ion collisions. *Adv. Nucl. Phys.* **25**, 1–205 (2000).
55. Acharya, S. et al. Unveiling the strong interaction among hadrons at the LHC. *Nature* **588**, 232–238 (2020); erratum **590**, E13 (2021).
56. Adamczyk, L. et al. ΛΛ correlation function in Au + Au collisions at $\sqrt{s_{NN}} = 200$ GeV. *Phys. Rev. Lett.* **114**, 022301 (2015).
57. Adam, J. et al. The proton-Ω correlation function in Au + Au collisions at $\sqrt{s_{NN}} = 200$ GeV. *Phys. Lett. B* **790**, 490–497 (2019).

STAR Collaboration

B. E. Aboona[1], J. Adam[2], L. Adamczyk[3], I. Aggarwal[4], M. M. Aggarwal[4], Z. Ahammed[5], A. K. Alshammri[6], E. C. Aschenauer[7], S. Aslam[8], J. Atchison[9], V. Bairathi[10], X. Bao[11], P. Barik[12], K. Barish[13], S. Behera[14], R. Bellwied[15], P. Bhagat[16], A. Bhasin[16], S. Bhatta[17], S. R. Bhosale[3], J. Bielcik[2], J. Bielcikova[2,18], J. D. Brandenburg[19], C. Broodo[15], X. Z. Cai[20], H. Caines[21], M. Calderó[22], D. Cebra[22], J. Ceska[2], I. Chakaberia[23], P. Chaloupka[2], Y. S. Chang[24], Z. Chang[25], A. Chatterjee[26], D. Chen[13], J. H. Chen[8], Q. Chen[27], W. Chen[8], Z. Chen[11], J. Cheng[28], Y. Cheng[29], W. Christie[7], X. Chu[7], S. Corey[19], H. J. Crawford[30], M. Csanád[31], G. Dale-Gau[2], A. Das[2], D. De Souza Lemos[7], I. M. Deppner[32], A. Deshpande[17], A. Dhamija[4], A. Dimri[17], P. Dixit[8], X. Dong[23], J. L. Drachenberg[9], E. Duckworth[6], J. C. Dunlop[7], Y. S. El-Feky[33], J. Engelage[30], G. Eppley[34], S. Esumi[35], O. Evdokimov[36], O. Eyser[7], B. Fan[37], R. Fatemi[38], S. Fazio[39], H. Feng[37], Y. Feng[37], E. Finch[40], Y. Fisyak[7], F. A. Flor[21], C. Fu[41], T. Fu[11], C. A. Gagliardi[1], T. Galatyuk[42], T. Gao[11], Y. Gao[8], G. Garcia[7], F. Geurts[34], A. Gibson[43], A. Giri[15], K. Gopal[14], X. Gou[11], D. Grosnick[43], A. Gu[44], J. Gu[8], A. Gupta[16], W. Guryn[7], A. Hamed[33], R. J. Hamilton[21], J. Han[37], X. Han[19], S. Harabasz[42], M. D. Harasty[22], J. W. Harris[21], H. Harrison-Smith[38], L. B. Havener[21], X. H. He[41], Y. He[11], N. Herrmann[32], L. Holub[2], C. Hu[45], Q. Hu[41], Y. Hu[23], H. Huang[46,47], H. Z. Huang[29], S. L. Huang[17], T. Huang[36], Y. Huang[31], Y. Huang[41], Y. Huang[8], M. Isshiki[35], W. W. Jacobs[25], A. Jalotra[16], C. Jena[14], A. Jentsch[7], Y. Ji[23], J. Jia[7,17], X. Jiang[37], C. Jin[34], Y. Jin[37], N. Jindal[19], X. Ju[48], E. G. Judd[30], S. Kabana[10], D. Kalinkin[38], J. Kang[49], K. Kang[28], A. R. Kanuganti[7], D. Kapukchyan[13], K. Kauder[7], D. Keane[6], M. Kesler[6], A. Khanal[50], Y. V. Khyzhniak[19], D. P. Kikoła[51], J. Kim[7], D. Kincses[31], I. Kisel[52], A. Kiselev[7], A. G. Knospe[53], J. Kołaś[51], B. Korodi[19], L. K. Kosarzewski[19], L. Kumar[4], M. C. Labonte[22], R. Lacey[17], J. M. Landgraf[7], C. Larson[38], J. Lauret[7], A. Lebedev[7], J. H. Lee[7], Y. H. Leung[32], C. Li[37], D. Li[48], H-S. Li[24], H. Li[54], H. Li[27], H. Li[37], W. Li[34], X. Li[48], X. Li[48], Y. Li[28], Z. Li[55], Z. Li[48], X. Liang[13], R. Licenik[2,18], T. Lin[11], Y. Lin[27], M. A. Lisa[19], C. Liu[41], G. Liu[55], H. Liu[44], L. Liu[37], L. Liu[8], Z. Liu[8], Z. Liu[37], T. Ljubicic[34], O. Lomicky[2], E. M. Loyd[13], T. Lu[41], J. Luo[48], X. F. Luo[37], L. Ma[8], R. Ma[7], Y. G. Ma[8], N. Magdy[56], D. Mallick[37], R. Manikandhan[15], C. Markert[57], O. Matonoha[2], K. Mi[45], S. Mioduszewski[1], B. Mohanty[58], B. Mondal[58], M. M. Mondal[59], I. Mooney[21], J. Mrazkova[2,18], M. I. Nagy[31], C. J. Naim[17], A. S. Nain[4], J. D. Nam[60], M. Nasim[12], H. Nasrulloh[48], J. M. Nelson[30], M. Nie[11], G. Nigmatkulov[36], T. Niida[35], T. Nonaka[35], G. Odyniec[23], A. Ogawa[7], S. Oh[49], K. Okubo[35], B. S. Page[7], S. Pal[2], A. Pandav[23], A. Panday[12], A. K. Pandey[51], T. Pani[61], A. Paul[13], S. Paul[17], D. Pawlowska[51], C. Perkins[30], S. Ping[8], J. Pluta[51], B. R. Pokhrel[60], I. D. Ponce Pinto[21], M. Posik[60], E. Pottebaum[21], S. Prodhan[14], T. L. Protzman[53], A. Prozorov[2], V. Prozorova[2], N. K. Pruthi[4], M. Przybycien[3], J. Putschke[50], Y. Qi[37], Z. Qin[28], H. Qiu[41], C. Racz[13], S. K. Radhakrishnan[6], A. Rana[4], R. L. Ray[57], R. Reed[53], C. W. Robertson[24], M. Robotkova[2,18], M. A. Rosales Aguilar[38], D. Roy[61], P. Roy Chowdhury[51], L. Ruan[7], A. K. Sahoo[12], N. R. Sahoo[14], H. Sako[35], S. Salur[61], S. S. Sambyal[16], J. K. Sandhu[53], S. Sato[35], B. C. Schaefer[53], N. Schmitz[62], F-J. Seck[42], J. Seger[63], R. Seto[13], P. Seyboth[62], N. Shah[64], P. V. Shanmuganathan[7], T. Shao[8], M. Sharma[16], N. Sharma[12], R. Sharma[14], S. R. Sharma[14], A. I. Sheikh[6], D. Shen[11], D. Y. Shen[41], K. Shen[48], S. Shi[37], Y. Shi[11], E. Shulga[7], F. Si[48], J. Singh[10], S. Singha[41], P. Sinha[14], M. J. Skoby[24,65], N. Smirnov[21], Y. Söhngen[32], Y. Song[21], T. D. S. Stanislaus[43], M. Stefaniak[19], Y. Su[48], M. Sumbera[18], X. Sun[41], Y. Sun[48], B. Surrow[60], M. Svoboda[2,18], Z. W. Sweger[22], A. C. Tamis[21], A. H. Tang[7], Z. Tang[48], T. Tarnowsky[66], J. H. Thomas[23], A. R. Timmins[15], D. Tlusty[63], D. Torres Valladares[34], S. Trentalange[29], P. Tribedy[7], S. K. Tripathy[51], T. Truhlar[2], B. A. Trzeciak[2], O. D. Tsai[7,29], C. Y. Tsang[6,7], Z. Tu[7]✉, J. E. Tyler[1], T. Ullrich[7], D. G. Underwood[43,67], G. Van Buren[7], J. Vanek[7]✉, I. Vassiliev[52], F. Videbæk[7], S. A. Voloshin[50], F. Wang[24], G. Wang[29], G. Wang[37], J. S. Wang[44], J. Wang[11], K. Wang[48], X. Wang[11], Y. Wang[48], Y. Wang[37], Y. Wang[28], Z. Wang[8], Z. Wang[11], Z. Y. Wang[8], A. J. Watroba[3], J. C. Webb[7], P. C. Weidenkaff[32], G. D. Westfall[66], D. Wielanek[51], H. Wieman[23], G. Wilks[36], S. W. Wissink[25], R. Witt[68], C. P. Wong[7], J. Wu[45], X. Wu[29], X. Wu[48], X. Wu[37], B. Xi[8], Y. Xiao[8], Z. G. Xiao[28], G. Xie[45], W. Xie[24], H. Xu[44], N. Xu[37], Q. H. Xu[11], Y. Xu[11], Y. Xu[8], Y. Xu[37], Y. Xu[41], Z. Xu[6], Z. Xu[67], G. Yan[11], Z. Yan[17], C. Yang[11], Q. Yang[11], S. Yang[55], Y. Yang[46,47], Z. Ye[55], Z. Ye[23], L. Yi[11], Y. Yu[11], H. Zbroszczyk[51], W. Zha[48], C. Zhang[8], D. Zhang[55], J. Zhang[11], L. Zhang[37], S. Zhang[69], W. Zhang[55], X. Zhang[41], Y. Zhang[41], Y. Zhang[48], Y. Zhang[11], Y. Zhang[27], Z. Zhang[7], Z. Zhang[36], F. Zhao[70], J. Zhao[8], S. Zhou[37], Y. Zhou[37], X. Zhu[28], M. Zurek[7,67] & M. Zyzak[52]

[1]Texas A&M University, College Station, TX, USA. [2]Faculty of Nuclear Sciences and Physical Engineering (FNSPE), Czech Technical University in Prague, Prague, Czech Republic. [3]Faculty of Physics and Applied Computer Science (FPACS), AGH University of Kraków, Kraków, Poland. [4]Panjab University, Chandigarh, India. [5]Variable Energy Cyclotron Centre, Kolkata, India. [6]Kent State University, Kent, OH, USA. [7]Brookhaven National Laboratory, Upton, NY, USA. [8]Fudan University, Shanghai, China. [9]Abilene Christian University, Abilene, TX, USA. [10]Instituto de Alta Investigación, Universidad de Tarapacá, Arica, Chile. [11]Shandong University, Qingdao, China. [12]Indian Institute of Science Education and Research (IISER), Berhampur, India. [13]University of California, Riverside, Riverside, CA, USA. [14]Indian Institute of Science Education and Research (IISER) Tirupati, Tirupati, India. [15]University of Houston, Houston, TX, USA. [16]University of Jammu, Jammu, India. [17]State University of New York, Stony Brook, NY, USA. [18]Nuclear Physics Institute of the CAS, Řež, Czech Republic. [19]The Ohio State University,

Columbus, OH, USA. [20]Shanghai Institute of Applied Physics, Chinese Academy of Sciences, Shanghai, China. [21]Yale University, New Haven, CT, USA. [22]University of California, Davis, Davis, CA, USA. [23]Lawrence Berkeley National Laboratory, Berkeley, CA, USA. [24]Purdue University, West Lafayette, IN, USA. [25]Indiana University, Bloomington, IN, USA. [26]National Institute of Technology, Durgapur, Durgapur, India. [27]Guangxi Normal University, Guilin, China. [28]Tsinghua University, Beijing, China. [29]University of California, Los Angeles, Los Angeles, CA, USA. [30]University of California, Berkeley, Berkeley, CA, USA. [31]Eötvös Loránd University (ELTE), Budapest, Hungary. [32]University of Heidelberg, Heidelberg, Germany. [33]American University in Cairo, New Cairo, Egypt. [34]Rice University, Houston, TX, USA. [35]University of Tsukuba, Tsukuba, Japan. [36]University of Illinois Chicago, Chicago, IL, USA. [37]Central China Normal University, Wuhan, China. [38]University of Kentucky, Lexington, KY, USA. [39]University of Calabria & INFN-Cosenza, Rende, Italy. [40]Southern Connecticut State University, New Haven, CT, USA. [41]Institute of Modern Physics, Chinese Academy of Sciences, Lanzhou, China. [42]Technische Universität Darmstadt, Darmstadt, Germany. [43]Valparaiso University, Valparaisoa, IN, USA. [44]Huzhou University, Huzhou, China. [45]University of Chinese Academy of Sciences, Beijing, China. [46]National Cheng Kung University, Tainan, Taiwan. [47]Academia Sinica, Nankang, Taipei, Taiwan. [48]University of Science and Technology of China, Hefei, China. [49]Sejong University, Seoul, South Korea. [50]Wayne State University, Detroit, MI, USA. [51]Warsaw University of Technology, Warsaw, Poland. [52]Frankfurt Institute for Advanced Studies (FIAS), Frankfurt, Germany. [53]Lehigh University, Bethlehem, PA, USA. [54]Wuhan University of Science and Technology, Wuhan, China. [55]South China Normal University, Guangzhou, China. [56]Texas Southern University, Houston, TX, USA. [57]University of Texas at Austin, Austin, TX, USA. [58]Homi Bhabha National Institute (HBNI), National Institute of Science Education and Research (NISER), Jatni, India. [59]Lovely Professional University, Phagwara, India. [60]Temple University, Philadelphia, PA, USA. [61]Rutgers University, Piscataway, NJ, USA. [62]Max-Planck-Institut für Physik, Munich, Germany. [63]Creighton University, Omaha, NE, USA. [64]Indian Institute of Technology, Patna, Patna, India. [65]Ball State University, Muncie, IN, USA. [66]Michigan State University, East Lansing, MI, USA. [67]Argonne National Laboratory, Lemont, IL, USA. [68]United States Naval Academy, Annapolis, MD, USA. [69]Chongqing University, Chongqing, China. [70]Lanzhou University, Lanzhou, China. ✉e-mail: zhoudunming@bnl.gov; jvanek@bnl.gov

Methods

Reconstruction of Λ hyperons

For reconstruction of Λ hyperons, the first step of the analysis is selection of pure samples of π^+, π^-, p and $\bar{p}$. The charged tracks are selected on the basis of their kinematics—transverse momentum $p_T = \sqrt{p_x^2 + p_y^2}$ and pseudorapidity $\eta \equiv -\ln(\tan(\vartheta/2))$—in which ϑ is the angle between the particle momentum and the positive direction of the proton beam (z axis), and their number of hit points inside the TPC ($N_{hits,TPC}$, $N_{max,TPC}$). These charged tracks are then identified on the basis of their energy loss in the TPC gas by limiting the $n\sigma$ variable, which quantifies the difference between the measured energy loss and the expected energy loss for the hypothesized particle type. The selected proton and pion candidates are then paired and the pair topology is constrained to identify Λ and $\bar{\Lambda}$ hyperon candidates.

The full selections on Λ reconstruction are summarized in Extended Data Table 1. Six topological selection variables are defined as follows: DCA_p, DCA_π, distance of the closest approach of the proton or pion track to the primary vertex; DCA_{pair}, distance of the closest approach of the proton and pion tracks; DCA_Λ, distance of the closest approach of Λ candidate to the primary vertex; L_{dec}, reconstructed decay length of the hyperon candidate; cosθ, cosine of the pointing angle θ, in which θ is measured between the reconstructed momentum and the vector connecting the primary vertex to the decay point.

Last, the K_S^0 candidates are reconstructed using a similar topological method. For details, see refs. 40,58.

Λ pairs signal extraction

To extract the signal of Λ candidates, two sets of distributions are filled for each of the Λ hyperon pairs.

First, an invariant mass, M_{inv}, distribution that includes an unlike-sign (US) $p\pi$ pair matched with a different US $p\pi$ pair from the same event is obtained. An example of this distribution for $\Lambda\bar{\Lambda}$ pair candidates is shown in Extended Data Fig. 1. The US–US M_{inv} distribution has three components: (1) the main peak, in which two pairs of $p\pi$ decayed from two Λ particles from the same event; (2) two ridges that correspond to a $p\pi$ pair from a Λ decay paired with a combinatorial background pair; (3) a continuum that originates from a combinatorial background $p\pi$ pair matched to a different background $p\pi$ pair.

Second, a M_{inv} distribution is constructed by a US $p\pi$ pair and a like-sign (LS) $p\pi$ pair. The US–LS mass distribution is to estimate the two background contributions. It is then subtracted from the US–US distribution, leaving an M_{inv} distribution containing only the Λ hyperon candidates. The subtracted M_{inv} distribution is subsequently fitted with a 2D Gaussian function. Only pairs within $\pm 2\sigma$ around the mean are selected for further analysis. The same selection procedure is repeated for K_S^0 mesons. All of the aforementioned distributions are constructed using four distinct particles.

Only Λ and $\bar{\Lambda}$ hyperon candidates that are at mid-rapidity ($|y| < 1$), with transverse momentum p_T within $0.5 < p_T < 5.0$ GeV c^{-1} are selected for the analysis. The average transverse momentum $\langle p_T \rangle$ of the reconstructed Λ hyperons is 1.35 GeV c^{-1} (for K_S^0 mesons, it is 1.14 GeV c^{-1}). Further in the analysis, the selected pairs are divided into groups based on their relative kinematics ($\Delta\phi$ and Δy). The numbers of selected signal hyperon pairs is summarized in Extended Data Table 2. The signal-to-background ratios (S/B) of the selected hyperon pairs do not heavily depend on this relative kinematics and are in the range $7 < S/B_{\Lambda\bar{\Lambda}} < 8$ for $\Lambda\bar{\Lambda}$ pairs and in the range $3 < S/B_{\Lambda\Lambda} < 4$ for both ΛΛ and $\bar{\Lambda}\bar{\Lambda}$ pairs.

ME correction

Before the correlation signal can be extracted, the raw dN/dcosθ^* distributions have to be corrected for detector acceptance loss and inefficiency. The dominant detector effect originates from the low-momentum cut-off on pion p_T. The correction is performed using the ME technique for all dN/dcosθ^* distributions, in which the basic assumption is that all detector effects relevant for the dN/dcosθ^* shape affect both the same-event (SE) and the ME in the same way. The ME pairs are defined analogously to the SE distributions, except each Λ ($\bar{\Lambda}$) in the pair originates from two different events. For example, for one $\Lambda\bar{\Lambda}$ SE pair, we use the Λ particle as a reference and loop over other events that have a $\bar{\Lambda}$ particle. (We also perform the reverse by using the $\bar{\Lambda}$ particle as reference). The ME pairs are selected such that their relative kinematics matches the SE pairs ($|\Delta p_T| < 0.1$ GeV c^{-1}, $|\Delta\phi| < 0.1$ and $|\Delta y| < 0.1$). This is essential in describing the detector effect because the relative kinematics of the SE hyperon pairs dictates the magnitude of the acceptance effect. To not create a bias that some SE pairs will find more ME counterparts than others owing to the relative kinematic selections, the ME pairs are weighted by the inverse of the number of times each SE pair is used.

After mixing particles (Λ or K_S^0) from different events, the ME distribution of dN/dcosθ^* can be used to apply as a correction to the SE distribution. First, the ME distributions are normalized to the same number of pairs as the SE. Then the SE distribution is divided by the ME distribution and the resulting, corrected, distribution is rescaled to the same statistics as the original, uncorrected, SE distribution.

This acceptance correction method was verified using simulated minimum-bias $p + p$ collisions at $\sqrt{s} = 200$ GeV generated by the PYTHIA 8.3 event generator in the default tune. This closure test was performed both for default PYTHIA 8.3, with no expected spin–spin correlation, as well as for PYTHIA 8.3 with an artificially introduced signal. The result was used as an estimate of the systematic uncertainty of the ME technique, discussed in the 'Systematic uncertainty' section.

Extracting spin correlation signal

After correcting the detector effects, the corrected dN/dcosθ^* distributions are fitted by equation (1) and the polarization parameter $P_{\Lambda_1\Lambda_2}$ is extracted. The quality of the fits was checked by calculating χ^2/NDF (NDF is number of degrees of freedom of the fit). The resulting fits all have similar χ^2/NDF values, with an average of $\chi^2/NDF = 0.7$ over all performed fits. The total and background-only dN/dcosθ^* distributions provide the spin correlation for a mixture of signal + background (P_{S+B}) and the background only (P_B), respectively. The signal polarization (P_S) is obtained by using the relation:

$$P_{S+B} = f_s \times P_S + (1 - f_s) \times P_B, \quad (2)$$

in which f_s and $1 - f_s$ are the signal and background fractions, respectively. All background contributions P_B were found to be consistent with zero. The same analysis procedure is performed for $K_S^0K_S^0$ pairs.

Systematic uncertainty

Different sources of systematic uncertainty on the spin correlation of Λ hyperon and K_S^0 pairs are considered. The low p_T cut-off on the pion momentum selection is varied from $p_T > 150$ MeV c^{-1} to $p_T > 170$ MeV c^{-1}, which results in an absolute systematic uncertainty of 0.010 in the extracted signal of $P_{\Lambda_1\Lambda_2}$. The systematic variation of the topological selection of the secondary vertex is modified from the default values $DCA_{pair} < 1.0$ cm, 2 cm $< L_{dec} <$ 25 cm and cos$\theta > 0.996$ to $DCA_{pair} < 0.9$ cm, 3 cm $< L_{dec} <$ 25 cm and cos$\theta > 0.997$. This leads to an absolute uncertainty of 0.013 in $P_{\Lambda_1\Lambda_2}$. Similarly, daughter topological selection was varied from $DCA_p > 0.1$ cm and $DCA_\pi > 0.3$ cm to $DCA_p > 0.2$ cm and $DCA_\pi >$ 0.4 cm, which gives an absolute systematic uncertainty of 0.001. The last selection criteria variation was done for DCA_Λ from the analysis value of $DCA_\Lambda < 1.0$ cm to $DCA_\Lambda < 0.8$ cm and $DCA_\Lambda < 1.2$ cm, which gives an absolute systematic uncertainty of 0.004. Another systematic uncertainty source comes from the ME correction for the detector effect. This is performed on the basis of a MC simulation using the PYTHIA 8.3 model. The ME-corrected $P_{\Lambda_1\Lambda_2}$ in PYTHIA 8.3, expected to be zero as there is no genuine spin correlation in the MC model, is checked against the null expectation. A residual polarization value of 0.014 is observed after the

ME correction, which is quoted as an absolute uncertainty. Finally, the uncertainties in the quoted values of the weak decay constants are propagated to the final results. The total systematic uncertainty is obtained by adding individual uncertainty sources in quadrature.

Calculations of the SU(6) and Burkardt–Jaffe models

On the basis of $p + p$ events at $\sqrt{s} = 200$ GeV generated using PYTHIA 8.2, filtered through the STAR detector simulation, we obtain the composition of all Λ particles in terms of primary Λs and their feed-down contributions. The dominant feed-down contribution is from Σ^0, which rapidly decays into $\Lambda + \gamma$. With this information, we make a total of six categories of Λ hyperon pairs, shown in Extended Data Fig. 2. The plotted percentage is the relative fraction of the total number of $\Lambda\overline{\Lambda}$ pairs that are predicted by the simulation.

We then calculate the maximum expected $\Lambda\overline{\Lambda}$ pair spin–spin correlation using the relative contributions from Extended Data Fig. 2 and the expected single Λ hyperon's polarizations based on the SU(6) and Burkardt–Jaffe models[27]. The single Λ hyperon polarization, depending on its parent, is summarized in Extended Data Table 3. To simplify the calculations, except for Σ^0, other feed-down contributions are roughly 57% and −37% for the SU(6) quark model and the Burkardt–Jaffe model, respectively. The maximum expected pair spin–spin correlation, based on these two models, is then calculated according to the following formula:

$$P_{\Lambda\overline{\Lambda},\mathrm{SU(6)/BJ}} = \frac{1}{3} \times \sum_i R_i P_{\Lambda,\mathrm{SU(6)/BJ}} P_{\overline{\Lambda},\mathrm{SU(6)/BJ}}, \quad (3)$$

in which R_i are the relative feed-down contributions of the $\Lambda\overline{\Lambda}$ pairs and $P_{\Lambda,\mathrm{SU(6)/BJ}}$ and $P_{\overline{\Lambda},\mathrm{SU(6)/BJ}}$ are the corresponding single Λ polarizations from Extended Data Table 3. The factor 1/3 comes from the maximum relative spin polarization given our experimental method[24]. We also assign an uncertainty on these values, which comes from the composition of different feed-down contributions in different kinematic regions. In this way, we have estimated the maximum expected spin–spin correlation from the SU(6) to be:

$$P_{\Lambda\overline{\Lambda},\mathrm{SU(6)}} = 0.096 \pm 0.004, \quad (4)$$

and similarly for the Burkardt–Jaffe model:

$$P_{\Lambda\overline{\Lambda},\mathrm{BJ}} = 0.015 \pm 0.002. \quad (5)$$

Also, we should note that the PYTHIA 8 MC model generally describes the hyperon productions in proton–proton collisions, whereas the specific intrinsic uncertainty on the feed-down estimate is unknown and thus not considered here.

Data availability

All raw data for this study were collected using the STAR detector at Brookhaven National Laboratory and are not available to the public. Derived data supporting the findings of this study are publicly available in the HEPData repository (https://www.hepdata.net/record/159491) or from the corresponding author on request.

Code availability

The codes to process raw data collected by the STAR detector are publicly available on GitHub (https://github.com/star-bnl). The codes to analyse the produced data are not publicly available.

58. The STAR Collaboration. Measurement of transverse polarization of Λ and $\overline{\Lambda}$ hyperons inside jets in *pp* collisions at $\sqrt{s} = 200$ GeV. Preprint at https://arxiv.org/abs/2509.17487 (2025).
59. Ellis, J., Kotzinian, A., Naumov, D. & Sapozhnikov, M. Longitudinal polarization of Λ and $\overline{\Lambda}$ hyperons in lepton–nucleon deep-inelastic scattering. *Eur. Phys. J. C* **52**, 283–294 (2007).

Acknowledgements We thank the RHIC Operations Group and SDCC at BNL, the NERSC at LBNL and the Open Science Grid Consortium for providing resources and support. This work was supported in part by the Office of Nuclear Physics in the U.S. DOE Office of Science, the U.S. National Science Foundation, National Natural Science Foundation of China, Chinese Academy of Sciences, the Ministry of Science and Technology of China and the Chinese Ministry of Education, NSTC Taipei, the National Research Foundation of Korea, Czech Science Foundation and Ministry of Education, Youth and Sports of the Czech Republic, Hungarian National Research, Development and Innovation Office, New National Excellence Programme of the Hungarian Ministry of Human Capacities, Department of Atomic Energy and Department of Science and Technology of the Government of India, the National Science Centre and WUT IDUB of Poland, German Bundesministerium für Bildung, Wissenschaft, Forschung und Technologie (BMBF), Helmholtz Association, Ministry of Education, Culture, Sports, Science and Technology (MEXT) and Japan Society for the Promotion of Science (JSPS).

Author contributions All authors have contributed to the publication, being variously involved in the design and construction of the detectors, in writing the software, calibrating subsystems, operating the detectors and acquiring data and, finally, analysing the processed data. The STAR Collaboration members discussed and approved the scientific results. This article was prepared by a subgroup of authors appointed by the STAR Collaboration and subjected to an internal collaboration-wide review process. All authors reviewed and approved the final version of the paper. All authors contributed to all research steps and writing of the paper.

Competing interests The authors declare no competing interests.

Additional information
Correspondence and requests for materials should be addressed to Z. Tu or J. Vanek.

Peer review information *Nature* thanks Roman Zwicky, who co-reviewed with Rafael Aoude, Yasmine Amhis and Christian Weiss for their contribution to the peer review of this work.

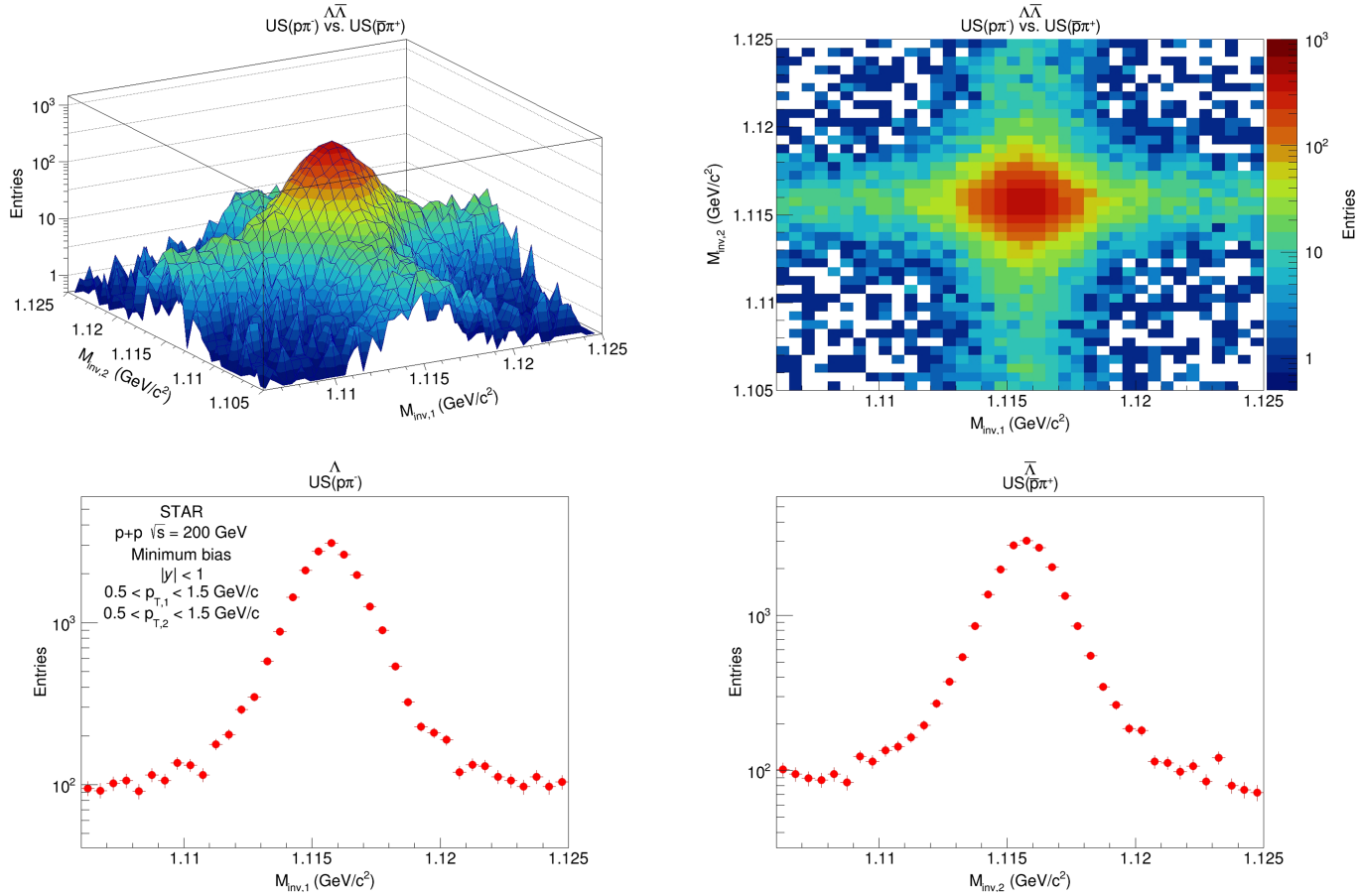

Extended Data Fig. 1 | 3D and 2D invariant mass distributions of $p\pi^-$ pairs, paired with $\bar{p}\,\pi^+$ pairs, are shown in the top-left and top-right panels, respectively. The projections of the multidimensional distributions to $p\pi^-$ and $\bar{p}\,\pi^+$ are shown in the bottom-left and bottom-right panels, respectively.

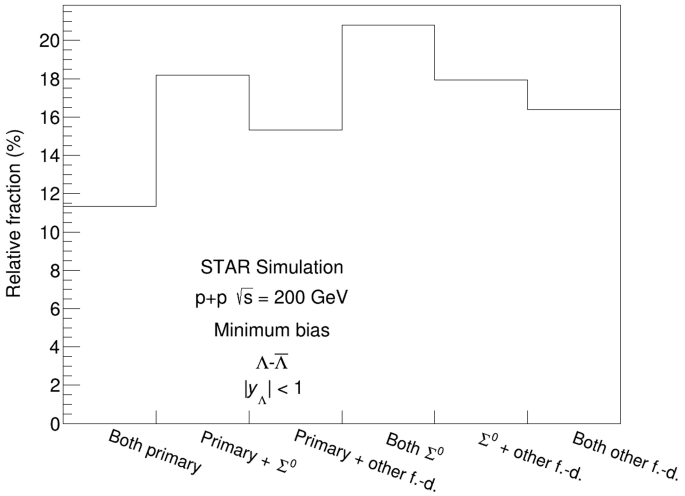

Extended Data Fig. 2 | Relative contribution to $\Lambda\overline{\Lambda}$ hyperon pair feed-down from PYTHIA 8.2 event generator events, which are simulated through the STAR detector. The Λ and $\overline{\Lambda}$ hyperons are selected using selection criteria from Extended Data Table 1. The pairs are divided into groups based on the origin of the single Λ ($\overline{\Lambda}$) hyperons in the pair: primary Λ, Λ from decay of Σ^0 and Λ from decay of any other hyperon species (labelled as 'other f.-d.' in the axis labels).

Extended Data Table 1 | Selection criteria for Λ and $\overline{\Lambda}$ hyperons. Reconstruction relies on track quality, proton and pion identification in the TPC, and the characteristic Λ decay topology

Track selection	$p_{\mathrm{T}} > 150\,\mathrm{MeV}/c$
	$\lvert\eta\rvert < 1$
	$N_{\mathrm{hits,TPC}} > 20$
	$N_{\mathrm{hits,TPC}}/N_{\mathrm{max,TPC}} > 0.52$
Particle identification	$\lvert n\sigma_{\pi}\rvert < 3$
	$\lvert n\sigma_{\mathrm{p}}\rvert < 2$
Λ topology	$DCA_{\pi} > 0.3\,\mathrm{cm}$
	$DCA_{\mathrm{p}} > 0.1\,\mathrm{cm}$
	$DCA_{\mathrm{pair}} < 1.0\,\mathrm{cm}$
	$DCA_{\Lambda} < 1.0\,\mathrm{cm}$
	$2\,\mathrm{cm} < L_{\mathrm{dec}} < 25\,\mathrm{cm}$
	$\cos\theta > 0.996$

Extended Data Table 2 | Counts of selected $\Lambda\bar{\Lambda}$, $\Lambda\Lambda$ and $\bar{\Lambda}\bar{\Lambda}$ signal pairs. Both short-range and long-range pairs included in the analysis are listed

Pair kinematics	$N_{\Lambda\bar{\Lambda}}$	$N_{\Lambda\Lambda}$	$N_{\bar{\Lambda}\bar{\Lambda}}$
$\lvert\Delta y\rvert < 0.5$, $\lvert\Delta\phi\rvert < \pi/3$	8,994	1,119	786
$\lvert\Delta y\rvert > 0.5$, or $\lvert\Delta\phi\rvert > \pi/3$	20,051	6,231	4,029

Extended Data Table 3 | Model predictions for Λ hyperon polarization. Shown are the expected *s* quark contributions from primary Λ production and the leading feed-down components in the SU(6) and Burkardt–Jaffe models. Values are taken from ref. 59

Λ's parent	SU(6)	Burkardt-Jaffe
s quark	1	0.63
Σ^0	1/9	0.15
Ξ^0	0.6	-0.37
Ξ^-	0.6	-0.37
Σ^*	5/9	N/A

Values are taken from ref. 59.